Electronic Supplementary Material (ESI) for Physical Chemistry Chemical Physics.

Unambiguous Hydrogenation of CO_2 by Coinage-Metal Hydride Anions: An Intuitive Idea Based on *In-Silico* Experiments

Md Habib[a], Ritabrata Sarkar[a], Santu Biswas[b], Anup Pramanik[b], Pranab Sarkar[b], Sougata Pal[*a]

[a]*Department of Chemistry, University of Gour Banga, Malda* - 732103*, India*

[b]*Department of Chemistry, Visva-Bharati University, Santiniketan - 731235, India*

Supporting Information

Table S1. Calculated thermochemical data for the activation and hydrogenation of CO_2 by AgH^- by using different levels of theory. All the energy values are presented in terms of free energy with zero-point energy correction at 298 K.

Level of theory	ΔG_{I1-I2} ***(kcal/mol)***	$\Delta G^{\ddagger}_{I1\rightarrow I2}$ ***(kcal/mol)***	ΔG_f ***(kcal/mol)***	$\Delta G^{\ddagger}_{I2\rightarrow I3}$ ***(kcal/mol)***
B3LYP/*6-311++G(3df, 2p)/SDD*	0.38	11.30	-3.57	2.30
B3LYP/*aug-ccpVTZ/SDD*	0.15	11.78	-3.49	2.31
B3LYP/*Def2TZVPP/SDD*	-0.43	10.43	0.80	2.19
CCSD/*6-311++G(3df, 2p)/SDD* [*]	-0.66	9.33	-23.50	0.64
PBE0/*6-311++G(3df, 2p)/SDD*	-0.04	12.12	-2.95	1.83
M06/*6-311++G(3df, 2p)/SDD*	0.71	9.95	-1.45	1.58
M05/*6-311++G(3df, 2p)/SDD*	1.24	9.87	-3.67	2.11
B2LYPD/*6-311++G(3df, 2p)/SDD*	-0.72	11.62	-3.43	1.21
TPSS/*6-311++G(3df, 2p)/SDD*	-2.53	14.42	-0.22	3.12
M06L/*6-311++G(3df, 2p)/SDD*	-1.65	10.72	3.27	1.99
BVP86/*6-311++G(3df, 2p)/SDD*	-1.09	13.56	1.44	3.78

[*]In this case single point energy calculations were performed based on the B3LYP-optimized geometries.

Table S2. Computed hydricities of the metal hydride species (MH^-) using different levels of theory.

Level of theory	ΔG_H^- (kcal/mol)		
	AuH^-	**AgH^-**	**CuH^-**
B3LYP/*6-311++G(3df, 2p)/SDD*	60.3	**43.2**	47.9
B3LYP/*aug-cc-pVTZ-PP*	61.5	**43.8**	46.8
PBE1PBE/ *aug-cc-pVTZ-PP*	64.4	**46.1**	51.2
M05/*aug-cc-pVTZ-PP*	54.1	**40.1**	44.6
TPSS/*aug-cc-pVTZ-PP*	66.5	**47.6**	54.8
BVP86/*aug-cc-pVTZ-PP*	67.5	**48.0**	54.6

Hydricity Calculation:

The thermodynamic hydricity[1-4] of a species, MH^- is defined as the free energy change (ΔG_H^-) of the reaction:

$$MH^- \longrightarrow M + H^-$$

The hydricity values have been computed by using B3LYP as density functional and 6-311G++(3df, 2p) as basis sets for the non-metals (C, O and H) and SDD basis sets for the metals (Cu, Ag, Au) with Stuttgart/Dresden (SDD) effective core potentials and these data have been presented in first row of Table S2. In rest of computations, aug-cc-pvtz basis set (C, H, O = all electron and aug-cc-pvtz-pp for Cu, Ag, Au with the relativistic effective core potential (ECP)) were used along with different density functionals. Very recently, a benchmark study has been performed on the calculation of hydricity of transition metal hydrides, MH^- (M= Sc-Zn).[5] The hydricity of CuH^- was predicted to be 52.4 kcal/mol by using B3LYP/aug-cc-pvtz level of theory. Our simulated data for CuH^- are in good agreement with the previous study. The hydricity value of AgH^- is found to be lower than the other hydrides, irrespective of the level of computation, indicating that AgH^- is more

hydridic in nature. In contrast, AuH^- is least hydridic among the systems of interest. Perhaps this is the first report of comparative study of hydride donor ability among the coinage metal hydrides. The gas phase computed hydricity value for most common and one of the strongest hydride donor BH_4^- molecule is 64.6 kcal/mol,[4] whereas it is 48.4 kcal/mol in THF solvent medium. In another study, such free energy values for the borane (BH_4^-) and alane (AlH_4^-) anions were reported to be 50 and 43 kcal/mol, respectively in acetonitrile solvent.[6] Thus, we claim that all MH^- are almost parallel with borane or alane with respect to hydride donor ability. Furthermore, the proposed hydride donor ability of AgH^- is predicted to be far better than the main group borane or alane hydrides.

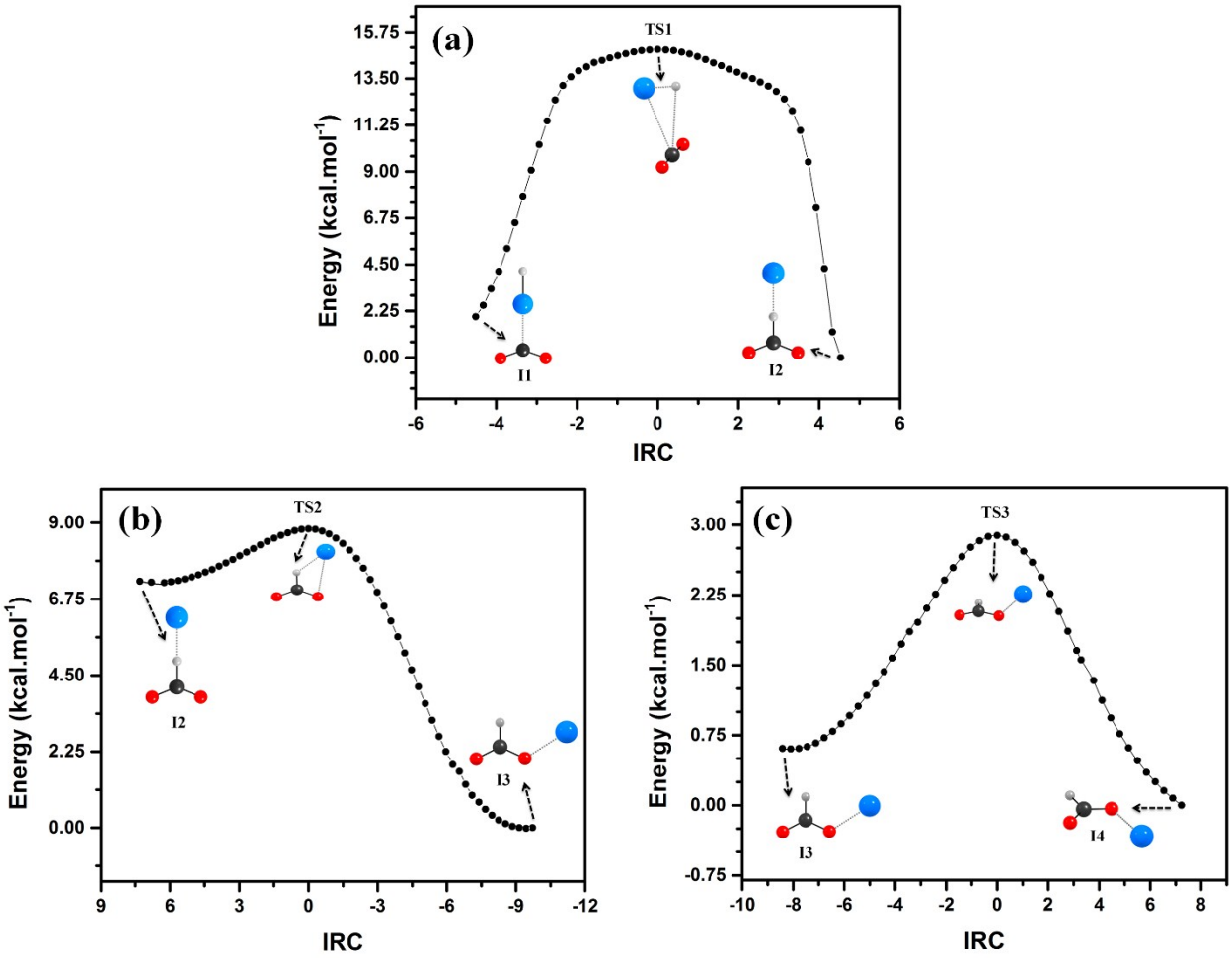

Figure S1. IRC plots of the TS structures (a-c for TS1-3, respectively) showing the connectivity of the respective intermediates. The calculations are done by using B3LYP/6-311G++(3df, 2p)/SDD level of theory.

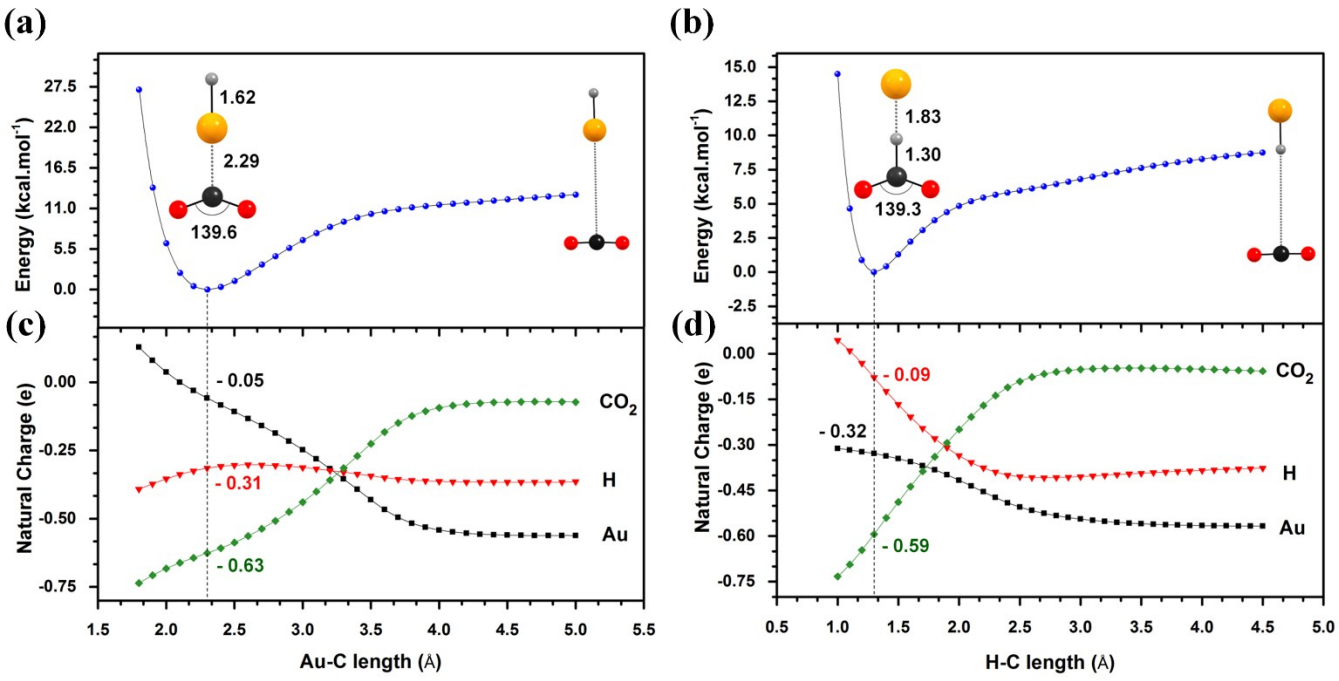

Figure S2. Relaxed potential energy surfaces with respect to (a) Au-C and (b) H-C bond lengths. The insets show the corresponding geometries at the minimum point indicating the optimized bond angle (°) and bond lengths (Å). Black, red, orange and white colored balls represent the C, O, Au and H atoms, respectively. (c) and (d) represent the calculated natural charges on the corresponding atoms as a function distance. The calculations are done by using B3LYP/6-311G++(3df, 2p)/SDD level of theory.

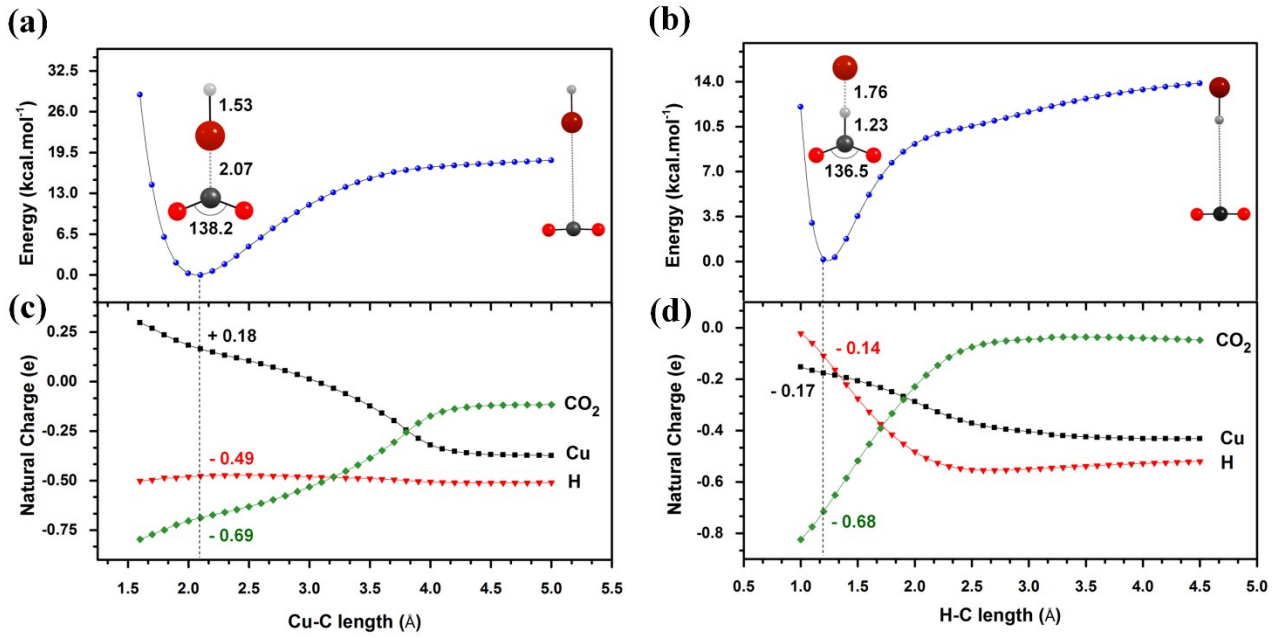

Figure S3. Relaxed potential energy surfaces with respect to (a) Cu-C and (b) H-C bond lengths. The insets show the corresponding geometries at the minimum point indicating the optimized bond angle (°) and bond lengths (Å). Black, red, brown and white colored balls represent the C, O, Cu and H atoms, respectively. (c) and (d) represent the calculated natural charges on the corresponding atoms as a function distance. The calculations are done by using B3LYP/6-311G++(3df, 2p)/SDD level of theory.

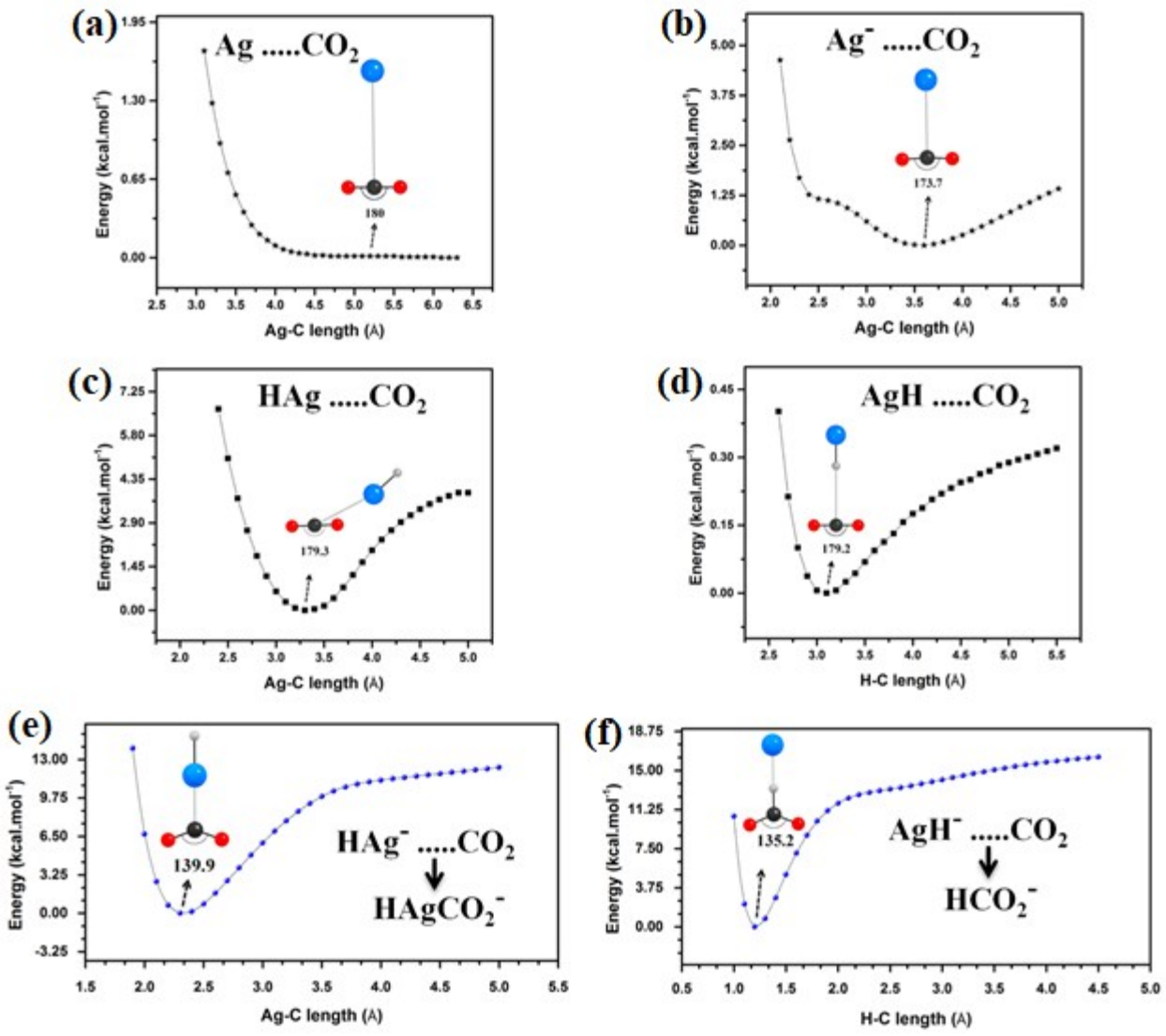

Figure S4. Relaxed potential energy surface (PES) plots with respect to Ag−C bond length for (a) Ag + CO_2, (b) Ag^- + CO_2. In both the cases, the equilibrium geometry is formed through a non-covalent interaction of metal with CO_2. Note that, an additional electron does not alter the nature of geometry, rather the geometry equilibrates at a shorter distance. (c) and (d) present similar PES plots with respect to Ag−C and H−C bond lengths, respectively for neutral AgH species. In each case, CO_2 molecule remains inactivated as indicated by the almost linear O-C-O bond angles of the respective systems. However, when an extra electron is added to AgH, the CO_2 molecules get activated as observed from the resultant O-C-O angle strains and the corresponding PESs, (e) and (f), respectively. When CO_2 interacts with AgH^- through H atom (f), the resulting complex is more stabilized than the other one. The insets show the corresponding geometries at the minimum point indicating the optimized bond angle (°) and bond lengths (Å).

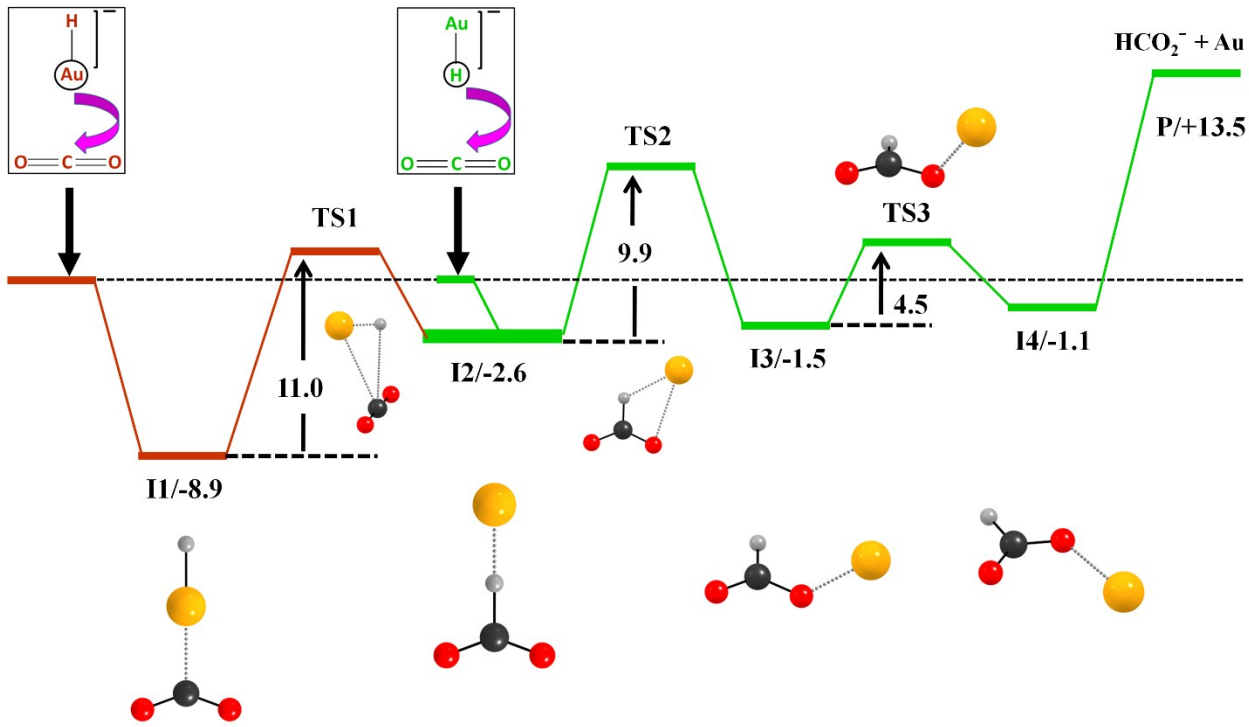

Figure S5. The calculated reaction pathways for the CO_2 activation followed by complete hydrogenation by AuH^-. The horizontal line corresponds to sum of energy of the reactants AuH^- and CO_2, fixed to zero. The relative free energies (in kcal/mol) of all the intermediates, transition states and product are shown with respect to the reactants. Both Path-A (activation by metal ion, brown line followed by green line) and Path-B (activation by hydride ion, green line) lead to the complete hydrogenation of the CO_2. Ease of formation of hydrogenated product HCO_2^- is facile for path A. The overall reaction for the formation of HCO_2^- is endergonic in nature. The calculations are performed by using B3LYP/6-311G++(3df, 2p)/SDD level of theory.

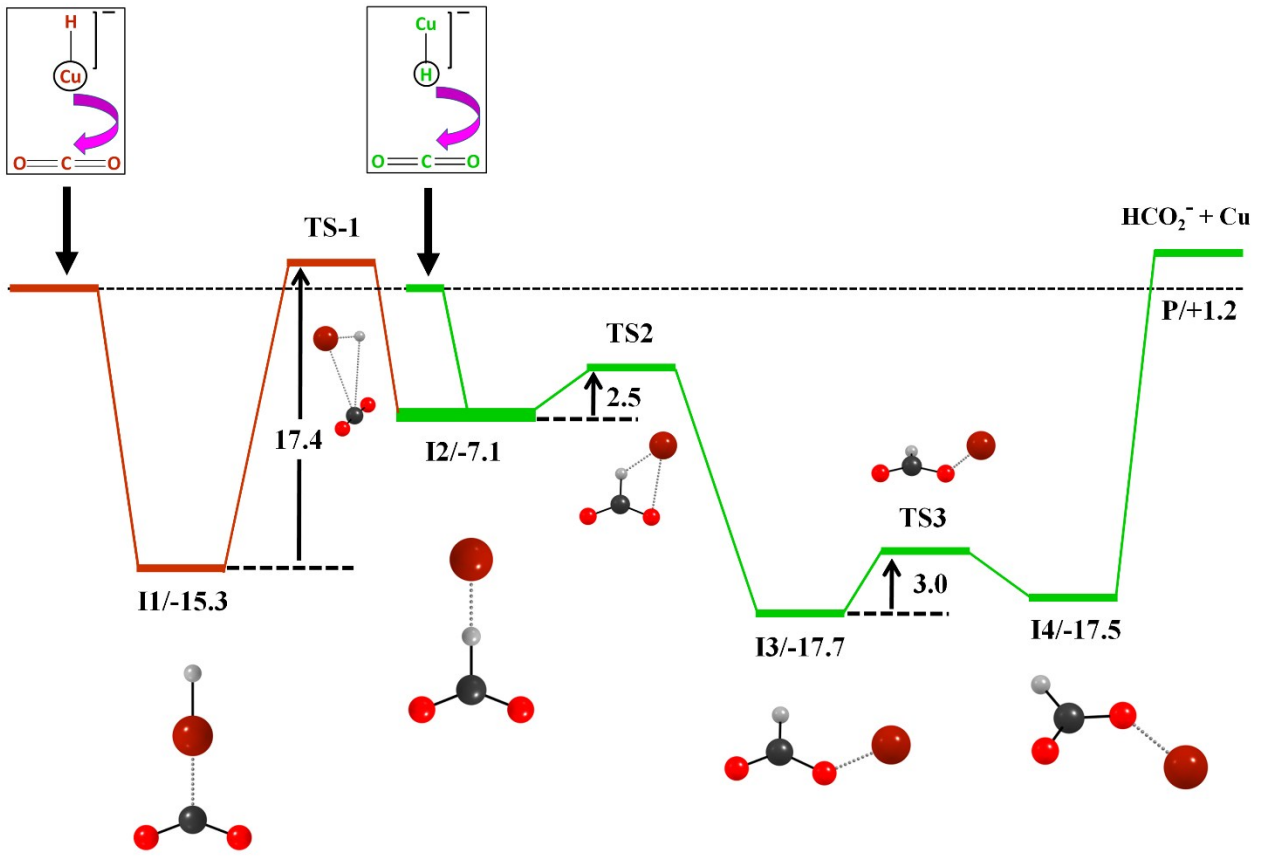

Figure S6. The calculated reaction pathways for the CO_2 activation followed by complete hydrogenation by CuH^-. The horizontal line corresponds to sum of energy of the reactants CuH^- and CO_2, fixed to zero. The relative free energies (in kcal/mol) of all the intermediates, transition states and product are shown with respect to the reactants. Both Path-A (activation by metal ion, brown line followed by green line) and Path-B (activation by hydride ion, green line) lead to the complete hydrogenation of the CO_2. Ease of formation of hydrogenated product HCO_2^- is facile for path A. The overall reaction for the formation of HCO_2^- is endergonic in nature. The calculations are performed by using B3LYP/6-311G++(3df, 2p)/SDD level of theory.

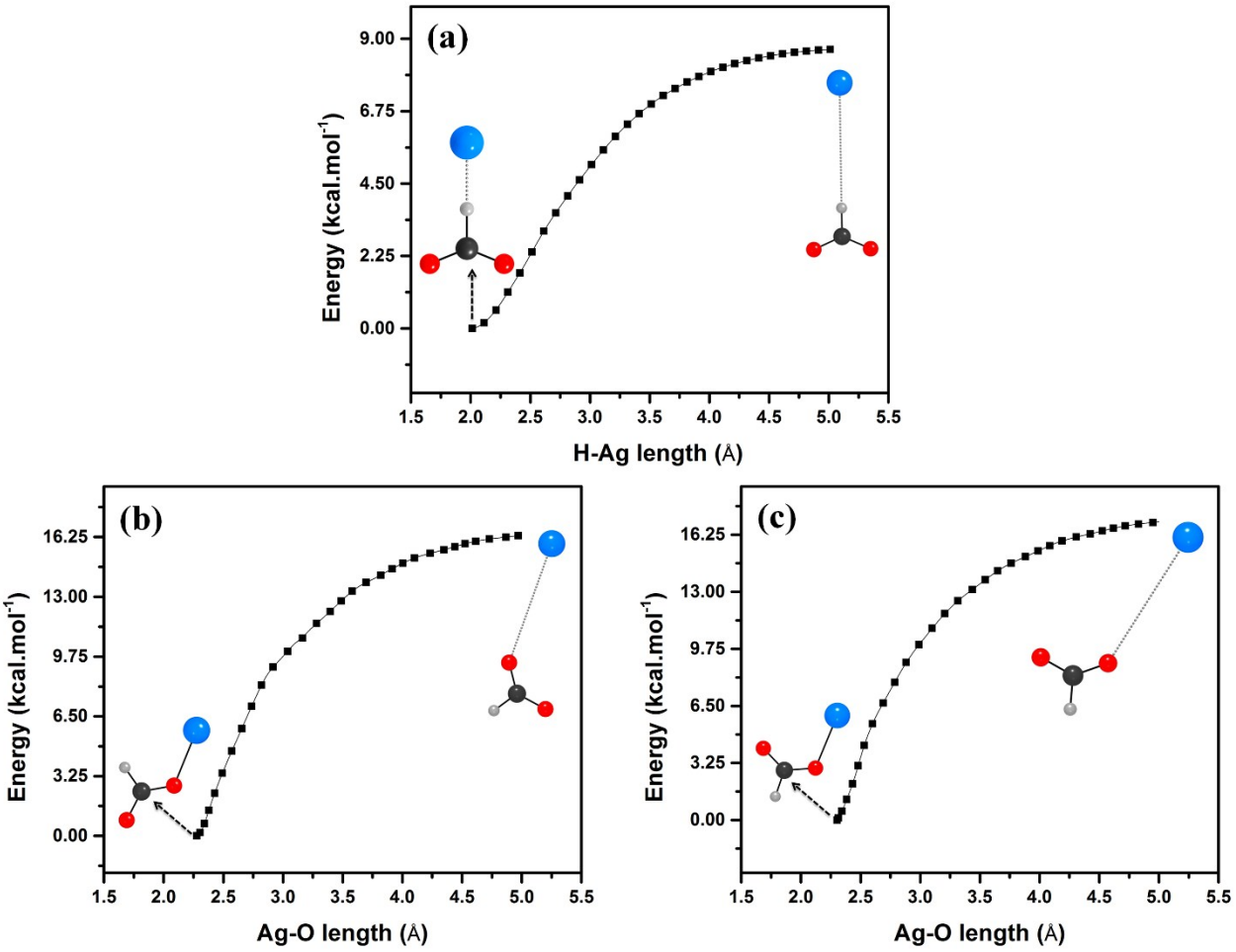

Figure S7. The relaxed potential energy surface scans during the formation of **P** from **I2** (a), **I3** (b), and **I4** (c). The scans were performed by fixing the H−Ag (a), and Ag−O bond lengths (in both b, c) while keeping rest of the nuclear coordinates relaxed. Note that, in each case, the final product is reachable because even after very long distances (5.0 Å), the energies of the respective species are still below that of the final product (**P**). Hence, we can say that direct conversion to final product from either (**I2, I3** or **I4**) is thermodynamically feasible.

References

1. A. Alherz, C.-H. Lim, J. T. Hynes and C. B. Musgrave, Predicting Hydride Donor Strength via Quantum Chemical Calculations of Hydride Transfer Activation Free Energy, *J. Phys. Chem. B*, 2018, 122, 1278-1288.
2. S. Ilic, U. Pandey Kadel, Y. Basdogan, J. A. Keith and K. D. Glusac, Thermodynamic Hydricities of Biomimetic Organic Hydride Donors, *J. Am. Chem. Soc.*, 2018, 140, 4569-4579.
3. K. M. Waldie, A. L. Ostericher, M. H. Reineke, A. F. Sasayama and C. P. Kubiak, Hydricity of Transition-Metal Hydrides: Thermodynamic Considerations for CO_2 Reduction, *ACS Catal.*, 2018, 8, 1313-1324.
4. J. Landmann, F. Keppner, D. B. Hofmann, J. A. Sprenger, M. Häring, S. H. Zottnick, K. Müller-Buschbaum, N. V. Ignat'ev and M. Finze, Deprotonation of a Hydridoborate Anion, *Angew. Chem. Int. Ed.*, 2017, 56, 2795-2799.
5. Y. Cai, X. Sun and X. Huang, Transition metal hydrides MH+/0/−(M= Sc− Zn): Benchmark study and periodic trends, *Comput. Theor. Chem.*, 2018, 1134, 15-21.
6. Z. M. Heiden and A. P. Lathem, Establishing the hydride donor abilities of main group hydrides, *Organometallics*, 2015, 34, 1818-1827.